RSC Advances

PAPER

Cite this: *RSC Adv.*, 2016, **6**, 8222

Operando Raman spectroscopic studies of lithium zirconates during CO_2 capture at high temperature†

Diana Peltzer, John Múnera and Laura Cornaglia*

Received 20th October 2015
Accepted 5th January 2016

DOI: 10.1039/c5ra21970a

www.rsc.org/advances

Li_2ZrO_3 based sorbents were synthesized for CO_2 capture at high temperature between 500 and 700 °C. Monoclinic ZrO_2, tetragonal Li_2ZrO_3, Li_2CO_3, K_2CO_3 and $LiKCO_3$ phases were detected by XRD and Raman spectroscopy. The sorbents showed high stability and moderate capture efficiency. The addition of K resulted in the improvement of capture efficiency from 0.052 g CO_2 g mat^{-1} in materials without K to 0.083 g CO_2 g mat^{-1} in the doped solid. Here, we report an experimental setup of Raman spectroscopy coupled with online mass spectrometry and a demonstration of its capabilities using lithium zirconates as sorbents for high temperature CO_2 capture. *Operando* Raman spectroscopy allowed us to follow up the phase evolution during the capture process for the first time. The results obtained confirmed the presence of molten K and Li carbonates when the K-doped zirconates were exposed to CO_2 at 500 °C.

1. Introduction

Today, the excess of GHG (Greenhouse Gases) emissions is a critical issue since their accumulation in the atmosphere is directly associated with the increase of the Earth's mean temperature. Among GHG, carbon dioxide (CO_2) plays a leading role because it contributes to 60 percent of the global warming effect, although other gases have much higher warming potential since they absorb more heat per molecule than carbon dioxide.[1] According to the IEA[2] (International Energy Agency), global emissions of carbon dioxide stood at 32.3 billion tons in 2014, unchanged from the preceding year but different projections predict an increase of CO_2 emissions until 2100, approximately.[3] Power plants, oil refineries, biogas sweetening as well as production of ammonia, ethylene oxide, cement and iron and steel are the main industrial sources of CO_2.[4,5] Among them, fuel burning in power plants for energy supply greatly contributes to CO_2 emission, and large efforts are being carried out to decrease it. In order to effectively reduce CO_2 emission into the atmosphere, carbon dioxide capture and storage (CCS) processes have been investigated. They include a wide range of technologies that associate capture, transport and storage of CO_2.[6] Three main strategies are generally available for CO_2 capture, namely post-combustion, pre-combustion, and oxyfuel combustion, and their specific application depends on the concentration of CO_2, gas pressure and type of fuel employed.[7] Among current strategies, post-combustion capture offers some advantages, *e.g.* lower costs by operation at the temperature of flue gases, which avoids additional costs for cooling or higher capture times; easy adaptation in assembled structures, *etc.* Moreover, it allows the use of materials that react reversibly with CO_2 depending on the operating conditions.[8]

Development of dry-based sorbents for CO_2 post-combustion capture is a promising alternative because they have several advantages with respect to the liquid solvents used at present. They are mostly organic and inorganic compounds and can be classified according to their sorption and desorption temperatures as low-temperature (<200 °C), intermediate-temperature (200–400 °C), and high-temperature (>400 °C) sorbents. Low-temperature sorbents include carbon, graphite–graphene, zeolite, Metal Organic Frameworks (MOF), silica and polymer based adsorbents. Intermediate-temperature acceptors are mostly layered double hydroxides (LDH) and MgO based sorbents. Finally, high-temperature sorbents are limited to CaO and alkali zirconates and silicate-based materials.[9,10] The latter capture CO_2 between 450 °C and 650 °C and generate alkali carbonates; then, by increasing temperature, the reversible reaction (decarbonation) could occur.[6,11] Among them, lithium zirconates and silicates have some advantages like high capture capacity, lower regeneration temperatures (<750 °C) compared to other high-temperature sorbents such as calcium oxide, and elevated stability, thus allowing operating for many cycles without loss of performance. These features make them promising alternatives for the capture process.[12] Moreover, Argentina is the second largest producer of lithium compounds and has the third biggest reserves of lithium worldwide, making the use

Instituto de Investigaciones en Catálisis y Petroquímica (INCAPE), Universidad Nacional del Litoral, Facultad de Ingeniería Química, Santiago del Estero 2829, 3000, Santa Fe, Argentina. E-mail: lmcornag@fiq.unl.edu.ar

† Electronic supplementary information (ESI) available. See DOI: 10.1039/c5ra21970a

of Li-based compounds very attractive to industry and academic research.[13] Even though lithium zirconates and silicates have low reaction rates, doping with alkaline metals like K or Na improves the kinetics of the capture process through the formation of melting salts at the reaction temperature, thus reducing the diffusive limitations of CO_2.[14–17]

Both the synthesis method and the starting reagents are determinants of sorbent capacity and kinetic properties. Ida *et al.*[14] reported the influence of particle size of precursors in Li_2ZrO_3 synthesized by the solid state method. Using low particle size starting ZrO_2, an enhancement in the kinetics of the carbonation reaction was obtained. Moreover, Radfarnia *et al.*[18] reported that Li_2ZrO_3-based sorbents synthesized by the ultrasound assisted method showed a higher capture capacity than the sorbents synthesized under the same conditions but without ultrasound. The simplicity of the synthesis method and the attainability of the starting reagents are also important in order to evaluate the scaling of processes for industrial applications. $LiNO_3$ is a soluble reagent with the advantages of safety, availability, and low melting point (600 °C).[8] Therefore, in the present study we synthesize Li_2ZrO_3-based materials by wet impregnation, a simple method which uses ZrO_2 and $LiNO_3$ as starting reagents and allows decreasing the calcination temperature needed to produce the Li_2ZrO_3 phase. The generated zirconates capture CO_2 over a range of temperatures and pressures through the "carbonation" reaction, which includes the transformation of zirconates into carbonates and zirconia. At temperatures above 650 °C, the reversible reaction can occur releasing the captured CO_2 and regenerating zirconate species. The evolution of the different generated phases could be followed using the *operando* Raman spectroscopy. This is a useful technique that combines the spectroscopic characterization of a material during reaction with the simultaneous measurement of activity. Raman spectroscopy is particularly suited for *in situ* studies because, given the fact that there is negligible interference from the gas phase, the Raman spectra may be acquired over a wide range of sample temperatures and pressures.[19]

The aim of this study was to develop lithium zirconates prepared by wet impregnation for CO_2 capture at high temperature. The influence of doping with K was also studied. *Operando* measurements were performed using Laser Raman spectroscopy coupled with online mass spectrometry, to simultaneously follow the evolution of the phases and monitor the capture process. Moreover, the solids were characterized by different techniques such as XRD, Laser Raman spectroscopy, XPS and surface area measurements.

2. Experimental

2.1. Sample synthesis

The samples were synthesized by wet impregnation of lithium and potassium soluble salts on a commercial ZrO_2, which during calcination could form the appropriate oxide. Starting materials were $LiNO_3 \cdot 2H_2O$ (Carlo Erba), ZrO_2 99% (MEL Chemicals) and KNO_3 (Aldrich).

The theoretical Li : Zr molar ratio required to form Li_2ZrO_3 is 2 : 1, which implies a weight proportion of 20% of Li_2O and 80% of ZrO_2. Then, a solid with 20 wt% of Li_2O was prepared, denoted $Li_2O(20)ZrO_2$. Specifically, for the preparation of this material, ZrO_2 was added to a $LiNO_3 \cdot 2H_2O$ solution (0.14 g mL^{-1}) keeping it under constant stirring at 70 °C until the sample resembled a wet paste. Then, the material was dried at 80 °C for 12 hours and calcined in air at 650 °C for 6 hours. A fraction of the calcined $Li_2O(20)ZrO_2$ was impregnated with a KNO_3 solution in order to obtain 5 wt% of K_2O on the previously synthesized material. The solid was denoted K-$Li_2O(20)ZrO_2$.

2.2. Sample characterization

BET measurements. BET measurements were performed in an automatic gas adsorption equipment (Micrometrics Gemini V). Prior to the measurements, samples were outgassed for 1 hour at 150 °C. Then, N_2 isotherms at −196 °C were executed.

XRD measurements. The X-ray diffraction patterns were recorded using a Shimadzu XD-D1 diffractometer, using Cu Kα ($\lambda = 1.542$ Å) radiation at 30 kV and 40 mA. The scan rate was 1–2° min^{-1} in the range $2\theta = 15$–80°.

CO_2 capture evaluation. The solids were evaluated in a conventional fixed-bed reactor, named "capture/desorption reactor". They were pretreated at 700 °C for 15 minutes in flowing N_2 to remove the carbonates formed during calcination and those produced under ambient conditions. After that, the capture/desorption cycles were carried out.

One capture/desorption cycle consists of four steps:

(i) Capture step: 60 minutes at 500 °C in 50% CO_2–50% N_2 mixture.

(ii) Desorption step: increasing temperature from 500 °C to 700 °C, 10 °C min^{-1}, in flowing N_2.

(iii) Regeneration step: 15 minutes at 700 °C in N_2 flow.

(iv) Cooling step: from 700 °C to 500 °C, 10 °C min^{-1}, in N_2 flow.

The total feed flow was always set at 60 mL min^{-1}. Flue gases (CO_2) and H_2 (35 mL min^{-1}) were fed into a methanation reactor and converted to methane by a nickel commercial catalyst operated at 400 °C. The resultant stream was continuously analyzed in an on-line FID detector (Shimadzu GC-8A Chromatograph).[20]

The mass of CO_2 captured per 1 gram of material during each cycle was calculated by the following equation:

$$\text{g } CO_2 \text{ per g mat} = \frac{A \times \text{MW } CO_2}{F \times \text{SW}}$$

where A is the signal area obtained by chromatography, MW CO_2 is the molecular weight of CO_2, F is the calibration factor of the chromatograph and SW is the sample weight in the capture reactor.

Laser Raman spectroscopy. Raman spectra were acquired in a LabRam (Horiba-Jobin-Yvon) spectrometer coupled to an Olympus confocal microscope (a 100× objective lens was used for simultaneous illumination and collection), equipped with a CCD detector cooled to about −70 °C using the Peltier effect and an 1800 l mm^{-1} diffraction grating. In all cases, the excitation wavelength was 532 nm (Spectra Physics diode pump solid state laser). Each Raman spectrum was collected for ~240

s and the laser power was set at 30 mW to avoid extensive laser heating. In all cases, the excitation wavelength was 532 nm (Spectra Physics diode pump solid state laser). The laser power was set at 30 mW. *In situ* measurements were carried out employing a cell (Linkam) coupled to the Raman system. The Raman spectra were curve-fitted using Lorentzian peaks after the baseline subtraction in the 400–700 cm^{-1} region.

The material was loaded in powder and the gases flowed through the solids. The fed mixtures were prepared in a flow system built for this purpose. The total flow was always 20 mL min^{-1}.

The following steps were carried out: pretreatment; at 700 °C for 15 minutes in flowing Ar; (i) capture step: 60 minutes at 500 °C in 30% CO_2–70% Ar mixture; (ii) desorption step: increasing temperature from 500 °C to 700 °C, 10 °C min^{-1}, in flowing Ar; (iii) regeneration step; 15 minutes at 700 °C in Ar flow and (iv) cooling step; from 700 °C to 500 °C, 10 °C min^{-1}, in Ar flow.

The gases at the outlet of the cell were analyzed by a quadrupole Dymaxion Dycor mass spectrometer from AMETEK. The spectrometer was assembled in our lab and it is equipped with a Pfeiffer HiCube™ ECO turbo pumping station with a dry diaphragm vacuum pump. The evolution of $m/z = 18$ (H_2O), 30 (NO) and 44 (CO_2) was analyzed during the experiments. A scheme of the *operando* Raman set-up is shown in Fig. 1.

XPS measurements. The XPS measurements were carried out using a multi-technique system (SPECS) equipped with a dual Mg/Al X-ray source and a hemispherical PHOIBOS 150 analyzer operating in the fixed analyzer transmission (FAT) mode. The spectra were obtained with a pass energy of 30 eV; a MgKα X-ray source was operated at 200 W and 12 kV. The working pressure in the analyzing chamber was less than 5.9×10^{-7} Pa. The XPS analyses were performed on the solids before and after the capture process. The spectral regions corresponding to Li 1s, K 2p, Zr 3d, Zr 3p, Zr 4s, O 1s and C 1s core levels were recorded for each sample. All photoelectron binding energies were referenced to the C 1s peak of adventitious carbon, set at 284.6 eV. The data treatment was performed with the Casa XPS program (Casa Software Ltd, UK). The peak areas were determined by integration employing a Shirley-type background. Peaks were considered to be a mixture of Gaussian and Lorentzian functions in a 70/30 ratio.

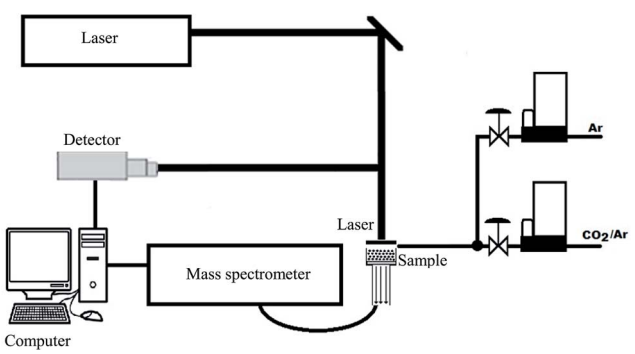

Fig. 1 Scheme of *operando* Raman system.

3. Results and discussion

3.1. Material characterization

XRD patterns of samples after calcination and before capture–desorption cycles (fresh) are exhibited in Fig. 2. They show tetragonal t-Li_2ZrO_3 formation after calcination at 650 °C (JCPDS-ICDD# 20-643) and the presence of unreacted monoclinic m-ZrO_2 (JCPDS-ICDD# 5-543). In addition to the diffraction peaks assigned to zirconia phases, reflections attributed to $LiKCO_3$ (JCPDS-ICDD# 34-1148), K_2CO_3 (JCPDS-ICDD# 1-1001) and Li_2CO_3 (JCPDS-ICDD# 1-996) phases were detected. On the other hand, the Raman spectra of K-$Li_2O(20)ZrO_2$, $Li_2O(20)ZrO_2$ and commercial Li_2CO_3 and K_2CO_3 included as reference, are shown in Fig. 3. The spectra for both sorbents show several bands corresponding to different vibrational modes of the ZrO_2 lattice.[21] Note that the starting ZrO_2 is in monoclinic phase since no peaks of tetragonal phase appear. Three clear signals corresponding to Li_2ZrO_3 can be visualized. The peak at 578 cm^{-1} corresponds to symmetrical stretching vibrations of Zr–O, lines at 380 cm^{-1} can be attributed to symmetrical stretching vibrations of Li–O bonds and the peak at 250 cm^{-1} corresponds to both stretching and bending vibrations of Zr–O bonds.[22] Both the XRD pattern and the Raman spectrum exhibit higher intensity peaks for t-Li_2ZrO_3 than ZrO_2 in the K-$Li_2O(20)ZrO_2$ sample.

In the case of K-$Li_2O(20)ZrO_2$, the Raman bands at 1090 cm^{-1} and 1050 cm^{-1} are assigned to a symmetric stretching of the C–O bonds in Li_2CO_3 and $LiKCO_3$, respectively.[23–25] Besides, a band corresponding to Li_2CO_3 appears below 200 cm^{-1}. The sharp signal at 126 cm^{-1} can be attributed to the contribution of several phases such as Li_2ZrO_3,[22] Li_2CO_3 (ref. 23 and 24) and K_2CO_3.[23] However, the $Li_2O(20)ZrO_2$ spectrum only shows a band at 1090 cm^{-1} assigned to Li_2CO_3. The carbonate species are formed by calcination in air atmosphere, which contains CO_2 traces. When the samples were calcined in ultrapure O_2–Ar atmosphere, no carbonate signals were detected (not shown).

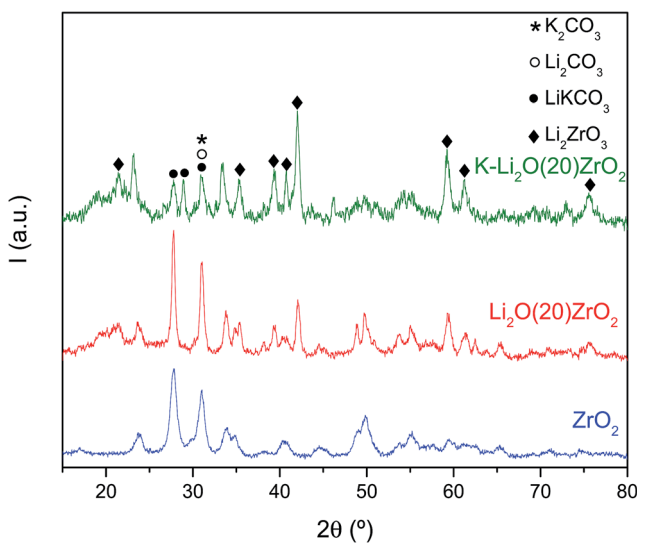

Fig. 2 DRX patterns of synthesized samples and ZrO_2.

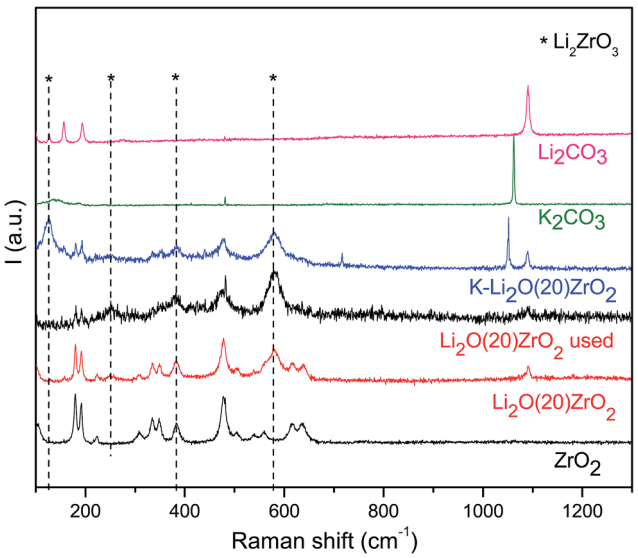

Fig. 3 Raman spectra of synthesized samples, m-ZrO_2, Li_2CO_3 and K_2CO_3. Li_2ZrO_3 bands are marked by dotted lines.

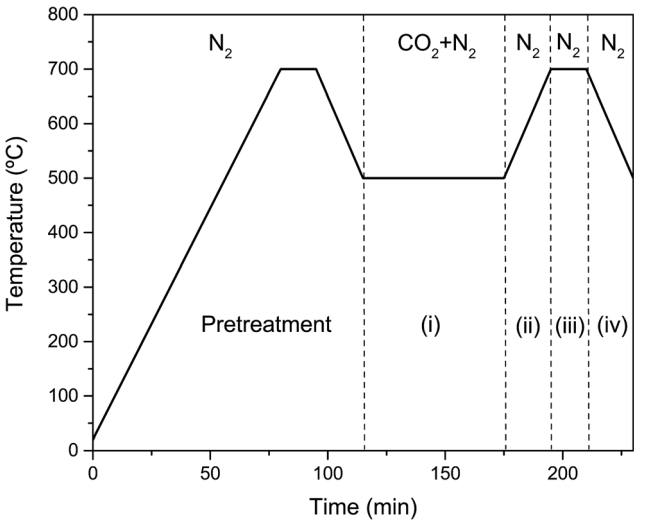

Fig. 4 Temperature and gases evolution during one capture/desorption cycle. Each cycle consists of four steps: capture (i), desorption (ii), regeneration (iii) and cooling (iv). Total flow: 60 mL min^{-1}. $P = 1$ atm.

The BET analysis shows that the surface areas of $Li_2O(20)ZrO_2$ and K-$Li_2O(20)ZrO_2$ are 10 $m^2\ g^{-1}$ and 4.5 $m^2\ g^{-1}$, respectively. However, the ZrO_2 precursor shows a surface area of 62.4 $m^2\ g^{-1}$. This decrease could be associated with ZrO_2 transformation into Li_2ZrO_3 at the calcination temperature employed. However, surface areas are higher than some materials synthesized by different methods such as soft chemistry and solid state reaction,[14,26,27] which show values no larger than 1 $m^2\ g^{-1}$.

3.2. Capture capacity evaluation

Both thermogravimetric analysis (TGA) and capture/desorption reactors are useful tools to investigate CO_2 sorbents at high temperatures. TGA is one of the most commonly used tools to determine the capacity of CO_2 sorption; however, TGA cannot be applied to accurately measure the absorption capacity of an acceptor because changes in weight may be caused by various factors. Capture/desorption reactors are more accurate systems since they directly measure released CO_2 on sorbents.[27] Therefore, in this study an assembled system which includes a fixed-bed reactor linked to a methanation reactor and a FID chromatograph was used for the CO_2 capture evaluation of different materials in capture/desorption cycles carried out between 500 and 700 °C.

Each cycle consists of four steps, namely capture (i), desorption (decarbonation) (ii), regeneration (iii) and cooling (iv). The system was fed with a CO_2 stream (50% CO_2–50% N_2 or 100% CO_2) at 500 °C during the capture step. In the other steps, the feed stream was always pure N_2 (Fig. 4). The integrated area in Fig. 5 allows calculating the mass of desorbed CO_2 during the decarbonation of each cycle.

Both materials showed excellent stability during 15 cycles (Fig. 6), even though a very slight decrease of the capture capacity can be observed in $Li_2O(20)ZrO_2$. This stability agreed with the Laser Raman phase analysis made before and after the capture/desorption cycles (Fig. 2), in which no significant changes were observed.

The average capture capacity of K-$Li_2O(20)ZrO_2$ was 0.083 g CO_2 g mat^{-1}, while the capture capacity of $Li_2O(20)ZrO_2$ was 0.052 g CO_2 g mat^{-1} when a 50% CO_2 mixture was fed. Previous studies concluded that K enhanced the capture kinetics. However, Ochoa *et al.*[27] reported that the addition of K_2O results in lower capacities and poorer stability due to particle coarsening, when Li_2ZrO_3 was prepared by the soft-chemistry route. Iwan *et al.*[29] reported that the reaction rate should be directly proportional to CO_2 pressure and could be expressed by $r = kp_{CO_2}{}^n$, where r is the rate of reaction, k is the rate constant, p_{CO_2}

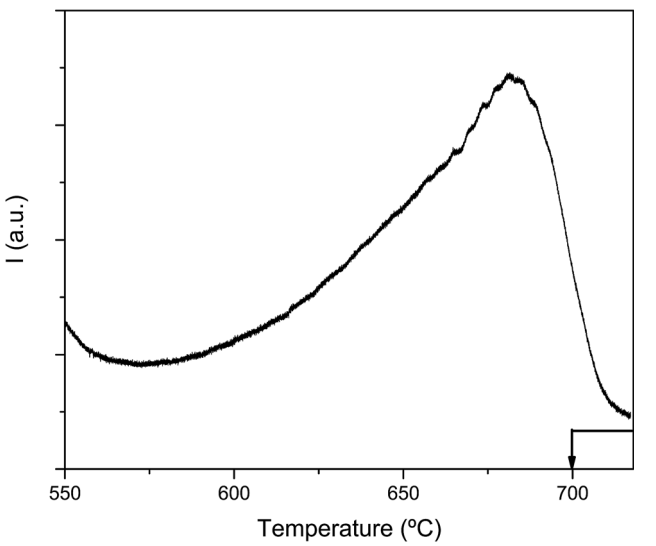

Fig. 5 CO_2 signal evolution during the desorption step in the first capture/desorption cycle for K-$Li_2O(20)ZrO_2$. Total flow: 60 mL min^{-1}. $P = 1$ atm. Heating rate: 10 °C min^{-1}.

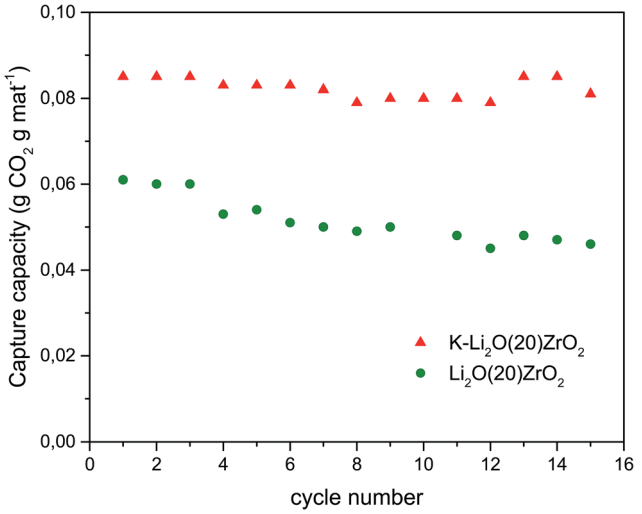

Fig. 6 Stability of materials represented by the evolution of capture capacity as a function of cycle number. All cycles were performed under the same conditions. Total flow: 60 mL min^{-1}. $P = 1$ atm.

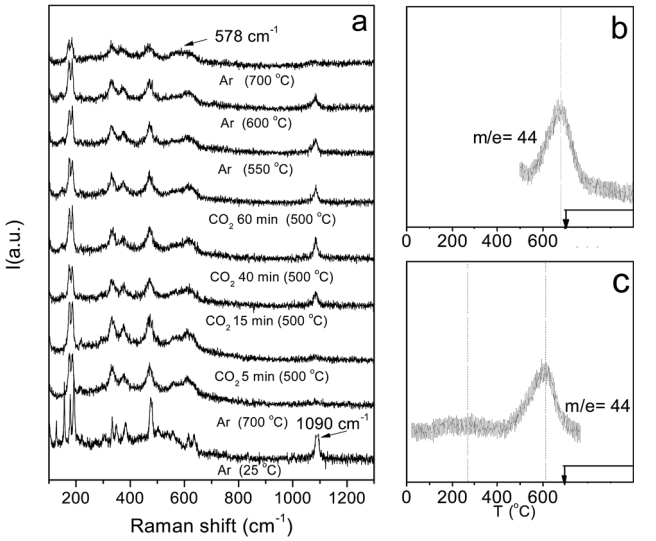

Fig. 7 *Operando* Raman spectroscopy of $Li_2O(20)ZrO_2$ during a complete/desorption cycle. (a) Raman spectra at different atmospheres and temperature conditions and (b and c) mass spectroscopy during the desorption step and pretreatment.

is the partial pressure of CO_2 in the gaseous phase and n is the order of reaction. In agreement with these results, when $Li_2O(20)ZrO_2$ was exposed to 100% CO_2 flow during the capture step, it showed a slight enhancement in capture capacity (0.074 g CO_2 g mat^{-1}). However, no increase was observed in K-$Li_2O(20)ZrO_2$ under the same conditions (0.082 g CO_2 g mat^{-1}). This fact could indicate that the K-doped material reached the maximum capacity capture with 50% CO_2 mixture, because of its enhanced kinetic reaction.[8]

3.3. Study of phase transformation by *operando* Raman spectroscopy during a CO_2 capture/desorption cycle

Several authors[11,14,27] have previously reported that Li_2ZrO_3 and molten carbonate species could be involved in the mechanism of the CO_2 capture at high temperature. Consequently, one the aims of this work is to study the presence of molten carbonates upon the reactivity of lithium zirconates during the capture/desorption cycle.

Operando characterization techniques are valuable tools to study the phase transformation of materials under genuine reaction conditions. For the *operando* measurements, a mass spectrometer assembled in our lab was employed. The evolution of m/z = 18 (H_2O), 30 (NO) and 44 (CO_2) was followed during the experiments.

Fig. 7 and 8 show the Raman spectra and gas evolution obtained during one capture/desorption cycle in the temperature range of 500–700 °C. The evolution of m-ZrO_2, Li_2CO_3, t-Li_2ZrO_3, K_2CO_3 and $LiKCO_3$ in $Li_2O(20)ZrO_2$ and K-$Li_2O(20)ZrO_2$ is presented. The Raman experiment included the same series of steps as the capture/desorption cycle, namely (i) capture, (ii) desorption, (iii) regeneration and (iv) cooling. Before the *operando* Raman experiment, a spectrum was taken at room temperature. In the case of the $Li_2O(20)ZrO_2$ material, the Raman spectrum between 200 and 650 cm^{-1} shows the presence of ZrO_2 monoclinic and a signal at 578 cm^{-1} assigned to symmetrical stretching vibrations of Zr–O bonds in Li_2ZrO_3 species.[21]

Besides the m-ZrO_2 and Li_2ZrO_3 bands, a signal at 1090 cm^{-1} assigned to Li carbonate could also be observed (Fig. 7a). In the case of the K-$Li_2O(20)ZrO_2$ material, a signal at 1051 cm^{-1} assigned to $LiKCO_3$ and/or K_2CO_3 was observed (Fig. 8a), in addition to the phases previously described. Prior to step (i), the samples were heated in Ar stream from 25 °C to 700 °C to decompose CO_3^{2-} species. Fig. 7b and 8b show the evolution of the mass spectrometer signals during the heating. For both

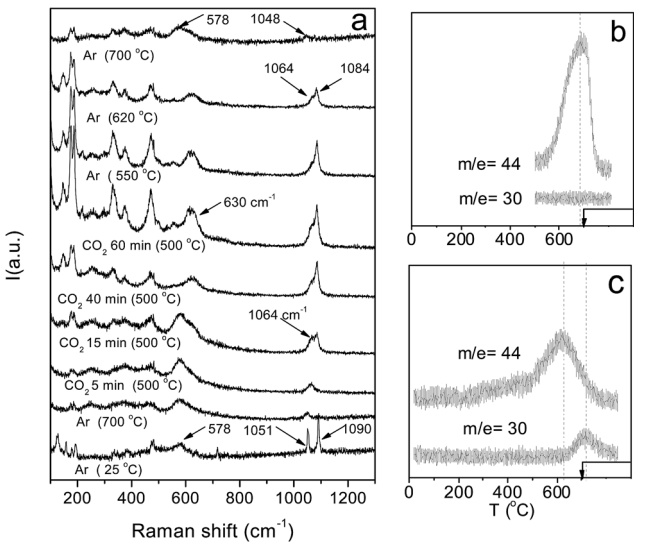

Fig. 8 *Operando* Raman spectroscopy of K-$Li_2O(20)ZrO_2$ during a complete/desorption cycle. (a) Raman spectra at different atmospheres and temperature conditions and (b and c) mass spectroscopy during the desorption step and pretreatment.

solids, it was observed that the CO_2 signal ($m/z = 44$) starts to increase slightly at temperatures above 270 °C, with a desorption peak maximum at 620 °C. This could correspond to decomposition of carbonate species formed during the preparation stage of the material probably due to the presence of CO_2 in the air used for calcination. Note that in addition to the $m/z = 44$, a signal corresponding to NO ($m/z = 30$) was observed in the K-doped solid due to the decomposition of residues of potassium nitrate.

For both solids (Fig. 7a and 8a), when the Raman band at 1090 cm^{-1} disappeared meaning that lithium carbonate decomposed, the main signal assigned to lithium zirconate increased (578 cm^{-1}). This observation is more remarkable for the K-doped solid. In this case, when the temperature reached 700 °C, the signal at 1050 cm^{-1} was still present. The evolution of Raman spectra as a function of time and temperature during the desorption step for the K-$Li_2O(20)ZrO_2$ sample was also included in Fig. 1 ESI.†

After heating, the temperature was decreased to 500 °C and the solids were subsequently exposed to a CO_2 (30%)/Ar mixture during 60 min (step (i)). Fig. 7a and 8a show the Raman spectra corresponding to the capture step performed at 500 °C at different exposure times. In the case of the $Li_2O(20)ZrO_2$ material after 15 min of CO_2 capture, the lithium carbonate in the solid phase (at 1090 cm^{-1}) was formed while the bands assigned to lithium zirconate decreased. On the other hand, in the Raman spectrum of the K-$Li_2O(20)ZrO_2$ sample after 5 min of CO_2 capture, there appeared two signals in the region of the CO_3^{2-}, located at 1064 and 1084 cm^{-1}. These signals increased with the exposure time at the same time as the ZrO_2 signals, while those assigned to Li_2ZrO_3 progressively decreased. The carbonate signals could be assigned to a molten Li_2CO_3–K_2CO_3 mixture and solid Li_2CO_3,[23] respectively. Note that according to the phase diagram of the Li_2CO_3–K_2CO_3 system reported by Ida and coworkers,[14] it is probable that at the potassium composition (K_2CO_3 molar fraction = 0.071) and temperatures (500–700 °C) used in this work, both carbonates are molten and Li_2CO_3 is also present in the solid phase.

Mizuhata *et al.*[30] studied the electrical conductivity and melting behavior of binary molten carbonate, $LiKCO_3$, coexisting with several kinds of metal oxide powder. They observed that the CO_3^{2-} stretching band in the Raman spectra was shifted toward a lower wavenumber from 1056 cm^{-1} to 1053 cm^{-1} with the decrease of the liquid phase for the system containing ZrO_2 powder and $LiKCO_3$ melted at 507 °C.

For both materials, during the desorption step (ii), the gas flow was turned to Ar and the temperature was again increased from 500 to 700 °C at a heating rate of 10° min^{-1}. Li_2CO_3 species, formed in the first stage (i), were decomposed at 700 °C (Fig. 7b and 8b). On the other hand, the signal at 1064 cm^{-1} was shifted toward a lower wavenumber at 1048 cm^{-1}, regenerating the solid for a new cycle. Taking into account the results reported by Mizuhata *et al.*[30] in the $LiKCO_3$ system containing ZrO_2 powder, this signal could be assigned to the $LiKCO_3$ molten phase.

Table 1 summarizes the different conditions and Raman signals present in each experiment. Note that in the $Li_2O(20)ZrO_2$ material, mainly Li_2ZrO_3 and Li_2CO_3 in the solid phase are present while in the K-$Li_2O(20)ZrO_2$ sample, carbonate species in the liquid phase are also observed.

In addition, to follow the transformation of Li_2ZrO_3 during the whole process, the Raman spectra were curve-fitted in the 400–700 cm^{-1} region using three Lorentzian peaks at 470, 578 and 630 cm^{-1}. The peaks at 470 and 630 cm^{-1} were assigned to ZrO_2 and the band at 578, to Li_2ZrO_3. The intensity ratios of bands at 578 and 470 cm^{-1} are summarized in Table 2. For the Ar treated K-$Li_2O(20)ZrO_2$ sample, the I_{578}/I_{470} ratio decreased during CO_2 capture, indicating the transformation of Li_2ZrO_3 into ZrO_2 and Li_2CO_3. Besides, the lower value presented for this sample, in comparison with the undoped one, is in agreement with its higher capture capacity. After desorption, the intensity ratio increased for both samples.

In general, for both solids, phase evolution is ruled by the carbonation reversible reaction. The thermodynamic study of this reaction predicts CO_2 capture taking place between 450 and 650 °C and at higher temperatures carbonate decomposition occurs, giving regenerate zirconates.[6,11]

$$Li_2ZrO_3(s) + CO_2(g) \rightarrow Li_2CO_3(s) + ZrO_2(s),\ 450\ ^\circ C < T < 650\ ^\circ C$$

$$Li_2CO_3(s) + ZrO_2(s) \rightarrow Li_2ZrO_3(s) + CO_2(g),\ T > 650\ ^\circ C$$

M. Olivares-Marín *et al.*[31] sustained that the introduction or doping of alkaline elements into Li_2ZrO_3 could apparently

Table 1 Species present in the samples exposed to different conditions, monitored by *in situ* Raman spectroscopy

	Samples	
Treatments	$Li_2O(20)ZrO_2$	K-$Li_2O(20)ZrO_2$
Ar, 25 °C	ZrO_2, Li_2CO_3	ZrO_2, Li_2ZrO_3, Li_2CO_3 and $LiKCO_3$
Ar, 700 °C	ZrO_2, Li_2ZrO_3	ZrO_2, Li_2ZrO_3 and molten $LiKCO_3$
CO_2 capture, 500 °C, 5 min	ZrO_2, Li_2ZrO_3, Li_2CO_3	ZrO_2, Li_2ZrO_3, molten Li_2CO_3–K_2CO_3 mixture and Li_2CO_3(s)
CO_2 capture, 500 °C, 15 min	ZrO_2, Li_2ZrO_3, Li_2CO_3	ZrO_2, Li_2ZrO_3, molten Li_2CO_3–K_2CO_3 mixture and Li_2CO_3(s)
CO_2 capture, 500 °C, 40 min	ZrO_2, Li_2ZrO_3, Li_2CO_3	ZrO_2, Li_2ZrO_3, molten Li_2CO_3–K_2CO_3 mixture and Li_2CO_3(s)
CO_2 capture, 500 °C, 60 min	ZrO_2, Li_2ZrO_3, Li_2CO_3	ZrO_2, Li_2ZrO_3, molten Li_2CO_3–K_2CO_3 mixture and Li_2CO_3(s)
Ar, 550 °C after CO_2 capture	ZrO_2, Li_2ZrO_3, Li_2CO_3	ZrO_2, Li_2ZrO_3, molten Li_2CO_3–K_2CO_3 mixture and Li_2CO_3(s)
Ar, 600 °C after CO_2 capture	ZrO_2, Li_2ZrO_3, Li_2CO_3	ZrO_2, Li_2ZrO_3, molten Li_2CO_3–K_2CO_3 mixture and Li_2CO_3(s)
Ar, 700 °C after CO_2 capture	ZrO_2, Li_2ZrO_3	ZrO_2, Li_2ZrO_3 and molten $LiKCO_3$

Table 2 Evolution of Li_2ZrO_3 intensity during Raman *operando* measurements

	I_{578}/I_{470}[a]	
Treatment	K-$Li_2O(20)ZrO_2$	$Li_2O(20)ZrO_2$
Ar, 700 °C	1.30	0.45
CO_2, 5 min, 500 °C	1.40	0.48
CO_2, 15 min, 500 °C	0.26	0.46
CO_2, 40 min, 500 °C	0.20	0.61
CO_2, 60 min, 500 °C	0.26	0.56
Ar, 550 °C	0.26	0.64
Ar, 620 °C	0.15	0.87
Ar, 700 °C	1.60	0.70

[a] Intensity ratios of bands at 578 and 470 cm^{-1}, assigned to Li_2ZrO_3 and ZrO_2, respectively.

change the melting points of the system and produce a liquid eutectic mixed-salt molten shell. The molten carbonate shell allows the diffusion and sorption of CO_2, which changes the viscoelastic properties of the sorbent and improves the effectiveness of the sorbent for the CO_2 uptake. It is generally accepted that doping with potassium favors the diffusion of CO_2 through the Li_2CO_3 layer formed on the surface during the capture reaction.[14,26,27,29] The layer in a totally or partially liquid phase at the reaction and regeneration conditions facilitates the diffusion of CO_3^{2-} and the mobility of K^+/Li^+ and O^{2-}. The increase in the mobility of the ions could influence the rate of the reactions. Therefore, the presence of liquid carbonate observed by Raman spectroscopy is in agreement with the higher capture capacity of the potassium doped material compared to the undoped sorbent. Then, the reaction mechanism would involve species in the liquid phase according to what was previously reported by Ochoa *et al.*[27]

$$CO_3^{2-}(liq) \rightarrow O^{2-}(liq) + CO_2(g)$$

$$O^{2-}(liq) + 2Li^+(liq) + ZrO_2(s) \rightarrow Li_2ZrO_3(s)$$

Operando Raman spectroscopy allowed us to follow up the phase evolution during the capture process for the first time. The results obtained helped us to confirm the reaction mechanism proposed for K-doped zirconates that would involve molten K and Li carbonates.

3.4. XPS analysis

XPS measurements were carried out in order to study surface changes in the materials during the capture process. The K-$Li_2O(20)ZrO_2$ and $Li_2O(20)ZrO_2$ samples were analyzed after different treatments: (a) pretreated (before the capture step), (b) with CO_2 capture (after the capture step and before the desorption step) and (c) used (after a whole capture/desorption cycle). The ZrO_2 precursor was also included in the XPS analysis as reference.

Table 3 summarizes the binding energy of the different elements. There were no significant differences in binding energies (BE) of C 1s, O 1s, Li 1s and K 2p regions in K-$Li_2O(20)ZrO_2$ and $Li_2O(20)ZrO_2$. However, BE in Zr 3p, 3d and 4s core levels are approximately 0.8 eV higher in ZrO_2 than in K-$Li_2O(20)ZrO_2$ and $Li_2O(20)ZrO_2$, which would suggest Li_2ZrO_3 surface phase formation. The Zr $3d_{5/2}$ core level BEs are shown in Table 3.

Changes in surface species were observed under different treatments. Fig. 9 shows the Li 1s–Zr 4s curve fitted XPS spectra for both samples. Signals at 55 eV and 52.6 eV correspond to Li 1s and Zr 4p, respectively. A satellite peak of Zr at lower BE was also included in order to improve the curve fitting of Li 1s and Zr 4s peaks. In $Li_2O(20)ZrO_2$ (Fig. 9a) the Li/Zr ratio was reversed as the complete capture process occurred, and the peak intensity of Li increased as the signal intensity of Zr 4s decreased. However, no significant changes in Li/Zr ratios were observed in the K-doped material (Fig. 9b).

The O 1s region shows two contributions at 532.0 and 529.8 eV assigned to carbonate oxygen (O_{CO_3}) and lattice oxygen ($O_{lattice}$), respectively. Differences in the intensities of $O_{lattice}$ and O_{CO_3} contributions are also illustrated in Fig. 2 ESI.† For both samples, $Li_2O(20)ZrO_2$ and K-$Li_2O(20)ZrO_2$, the O_{CO_3} peak intensity increased during the capture step and then decreased. However, this behavior was more marked in the K-doped sample. Moreover, no contribution of surface $O_{lattice}$ was observed in the latter after the capture step, which would agree with the higher capture capacity of this material. Furthermore, the analysis of the C 1s region shows the contribution of different carbon species, among them C_{CO_3} peaks at 289.4 ± 0.2 eV. These signals are in agreement with the results obtained in the O 1s region. Table 4 summarizes the surface atomic concentration of each material after the different treatments. For both materials, an increase in intensity of C_{CO_3} signals was

Table 3 Binding Energies (eV) of all elements in K-doped and undoped samples under different treatments

	Li 1s	K $2p_{3/2}$	Zr $3d_{5/2}$	$O_{lattice}$[a] 1s	O_{CO_3}[b] 1s	C_{CO_3}[b] 1s
Pretreated[c] K-$Li_2O(20)ZrO_2$	54.9	293.1	181.7	529.8	531.7	288.6
With capture[d] K-$Li_2O(20)ZrO_2$	54.9	293.0	181.9	—	531.4	288.8
Used[e] K-$Li_2O(20)ZrO_2$	54.9	293.2	181.7	530.0	532.0	288.8
Pretreated[c] $Li_2O(20)ZrO_2$	55.3	—	181.8	529.7	531.7	288.9
With[d] capture $Li_2O(20)ZrO_2$	55.1	—	181.8	529.6	531.7	289.3
Used[e] $Li_2O(20)ZrO_2$	55.1	—	181.7	529.7	531.9	289.3
ZrO_2	—	—	182.5	530.6	532.6	288.6
Used[e] $Li_2O(20)ZrO_2$[f]	55.0	—	181.7	529.3	531.8	289.4

[a] Oxygen corresponding to zirconia and lithium zirconate lattice. [b] Oxygen or carbon corresponding to carbonate species. [c] Before capture step. [d] After capture step and before desorption step. [e] Before a complete "capture–desorption" cycle. [f] Sample calcined under oxygen atmosphere.

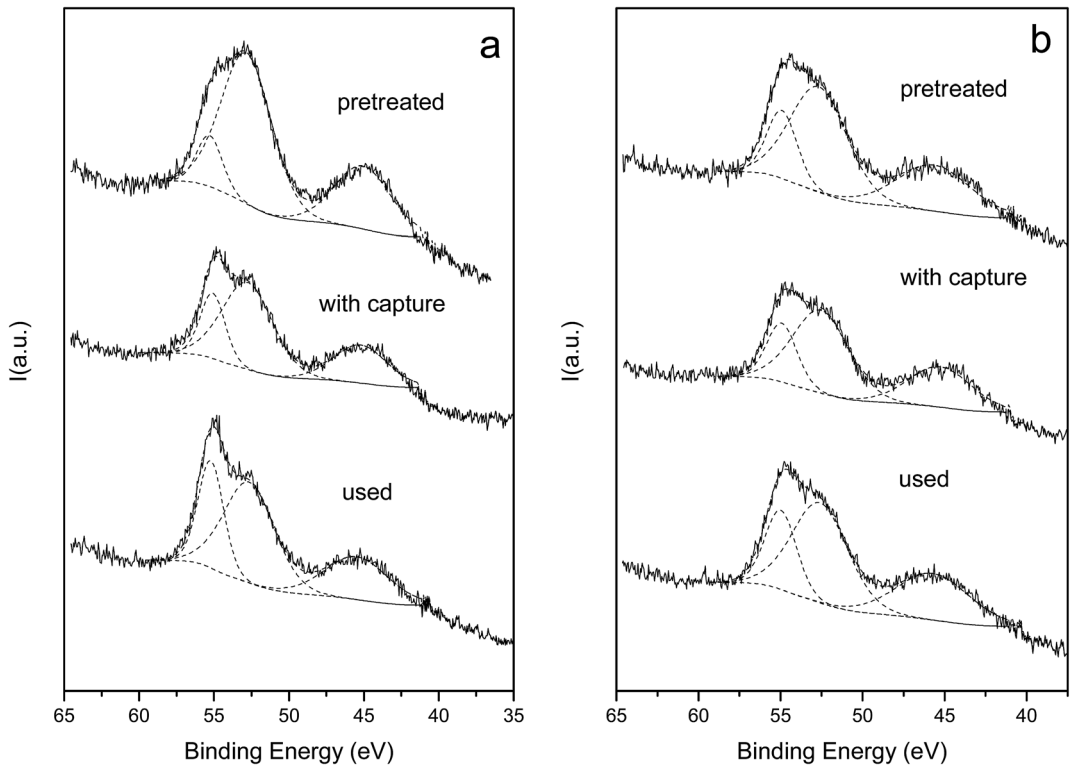

Fig. 9 XPS spectra of Li 1s and Zr 4p in $Li_2O(20)ZrO_2$ (a) and K-$Li_2O(20)ZrO_2$ (b) under different treatments: before the capture step, after the capture step and before the desorption step and after a complete capture/desorption cycle.

observed during the capture step; however, this increase was more pronounced in the K doped-material.

It can be observed that in the K-doped sample with CO_2 capture, both K and Zr atomic percentages decreased while C and O_{CO_3} concentration increased, and returned to the original values after the capture/desorption cycle. However, the Li concentration remained approximately constant. Moreover, in the undoped materials Zr concentration progressively decreased while C, Li and O_{CO_3} atomic percentages gradually increased.

Some trends are more clearly visualized using elemental ratios calculated from surface concentrations. The stoichiometric C/O ratio for CO_3^{2-} species should be equal to 0.33. In samples without K, the C/O ratio remained always near this value; however, in the K-doped materials values not above 0.19 were observed. Moreover, an increase of C/O ratio was noticed after the capture step, from 0.16 to 0.19. This fact would indicate the formation of CO_3^{2-} species during the capture process.

Both Li/Zr and C/Zr ratios were in the same order in K-doped and undoped materials but they showed different trends. In both samples, C/Zr ratios were very similar and increased after the CO_2 capture step. The K-doped sorbent showed a different behavior with respect to the undoped sorbent in the used samples, with a significantly lower C/Zr ratio than the latter. For the K-doped material, it can be observed that the C/Zr ratio increases and then recovers the original value after the "capture–desorption" cycle (0.51, 1.19 and 0.36 in the samples pretreated, with CO_2 capture and used, respectively). However,

Table 4 Elemental composition and atomic ratio of materials under different treatments

	%Li	%Zr	%K	$\%O_{CO_3}$ [a]	$\%O_{lattice}$ [b]	$\%C_{CO_3}$ [a]	C/O	Li/Zr	C/Zr
Pretreated[c] K-$Li_2O(20)ZrO_2$	18.5	12.6	4.6	40.0	17.8	6.4	0.16	1.46	0.51
With capture[d] K-$Li_2O(20)ZrO_2$	17.4	9.6	2.4	59.1	—	11.5	0.19	1.80	1.19
Used[e] K-$Li_2O(20)ZrO_2$	22.2	11.8	4.9	33.5	23.4	4.2	0.13	1.88	0.36
Pretreated[c] $Li_2O(20)ZrO_2$	12.7	21.6	—	29.6	30.4	9.6	0.32	0.71	0.54
With capture[d] $Li_2O(20)ZrO_2$	20.9	11.1	—	43.9	11.1	13.1	0.30	1.89	1.18
Used[e] $Li_2O(20)ZrO_2$	29.2	9.7	—	37.6	12.7	10.9	0.29	3.01	1.12
ZrO_2	—	25.6	—	24.5	40.1	9.7	0.40	—	0.38
Used[e] $Li_2O(20)ZrO_2$[f]	30.1	6.0	—	47.0	4.6	12.3	0.26	5.03	2.06

[a] Oxygen or carbon corresponding to carbonate species. [b] Oxygen corresponding to zirconia and lithium zirconate lattice. [c] Before capture step. [d] After capture step and before desorption step. [e] Before a complete "capture–desorption" cycle. [f] Sample calcined under oxygen atmosphere.

for the undoped material, the C/Zr ratio remained similar in the used and after CO_2 capture samples (0.54, 1.18 and 1.12). The ability of the K-doped material to recover the low C/Zr values could also be associated with a higher capture capacity, as verified by capture evaluation.

On the other hand, both materials showed a progressive increase of the Li/Zr ratio (pretreated < with CO_2 capture < used). However, this growth was much less pronounced in the K-doped sample than in the undoped material (from 1.46 to 1.88 and from 0.71 to 3.01 in K-doped and undoped samples, respectively). Note that Li/Zr and $O_{lattice}$/Zr ratios were higher in the K-doped than in the undoped pretreated materials. Furthermore, the Li/Zr ratio was close to the bulk composition (Li/Zr theoretical ratio = 2), which agrees with the high proportion of the Li_2ZrO_3 phase observed in Laser Raman spectroscopy studies.

A surface lithium segregation was observed in the used $Li_2O(20)ZrO_2$ sample (Li/Zr ratio = 3.01). The larger surface amount of Li observed in Li_xZrO_y prepared by soft-chemistry[28] have been explained by the lower surface free energy of lithium.

4. Conclusions

K-$Li_2O(20)ZrO_2$ and $Li_2O(20)ZrO_2$ sorbents were synthesized by wet impregnation using $LiNO_3$ and monoclinic ZrO_2.

XRD and Laser Raman spectroscopy characterization confirmed the presence of m-ZrO_2, t-Li_2ZrO_3, $KLiCO_3$, K_2CO_3 and Li_2CO_3 phases. Both solids showed a moderate capture efficiency, while K-$Li_2O(20)ZrO_2$ was slightly better than the undoped material. Moreover, they were stable during almost 15 cycles of capture/desorption.

Using *operando* Raman spectroscopy, we analyzed the phase behavior during the capture process and observed that it agreed well with the reversible carbonation reaction.

In the $Li_2O(20)ZrO_2$ sorbent, ZrO_2, Li_2CO_3 and Li_2ZrO_3 in the solid phase were present while in K-$Li_2O(20)ZrO_2$, carbonate species were molten and a fraction of Li_2CO_3 was also present in the solid phase.

The presence of molten $KLiCO_3$, K_2CO_3 and Li_2CO_3 carbonates during the CO_2 treatment at 500 °C was verified, supporting the role of ion mobility in the reaction rates. In addition, the positive influence of potassium-doping on the reactivity of lithium zirconate to ZrO_2 was confirmed for the first time under *operando* conditions.

The application of Raman spectroscopy in *operando* during the capture/desorption cycle allowed us to clearly follow the changes that occur simultaneously in the course of the different cycle steps and shows a high potential to study other high temperature sorbents under real conditions.

Acknowledgements

The authors wish to acknowledge the financial support received from UNL, CONICET and ANPCyT. Thanks are also given to ANPCyT for the purchase of the Raman instrument (PME 87-PAE 36985) and the UHV Multi Analysis System (PME 8-2003), and to Fernanda Mori for the XPS measurements. The support from Ana Tarditi and Betina Faroldi is also greatly appreciated.

References

1 A. Yamasaki, *J. Chem. Eng. Jpn.*, 2003, **36**, 361–375.
2 Energy and Climate Change, http://www.iea.org/publications/freepublications/publication/WEO2015SpecialReportonEnergyandClimateChange.pdf, accessed September 2015.
3 S. Mohr, J. Wang, G. Ellem, J. Ward and D. Giurco, *Fuel*, 2015, **141**, 120–135.
4 Carbon capture and utilization in the green economy, using CO_2 to manufacture fuel, chemicals and materials, http://www.policyinnovations.org/ideas/policy_library/data/01612/_res/id=sa_File1/CCU.pdf, accessed September 2015.
5 Trends in global CO_2 emissions, 2013 Report, http://edgar.jrc.ec.europa.eu/news_docs/pbl-2013-trends-in-global-co2-emissions-2013-report-1148.pdf, accessed September 2015.
6 Z. Lee, K. Lee, S. Bhatia and A. Mohamed, *Renewable Sustainable Energy Rev.*, 2012, **16**, 2599–2609.
7 M. Olivares-Marín and M. Maroto-Valer, *Greenhouse Gases: Sci. Technol.*, 2012, **2**, 20–35.
8 S. Wang, C. An and Q. Zhang, *J. Mater. Chem. A*, 2013, **1**, 3540–3550.
9 S. D. Kenarsari, D. Yang, G. Jiang, S. Zhang, J. Wang, A. G. Russell, Q. Wei and M. Fan, *RSC Adv.*, 2013, **3**, 22739–22773.
10 J. Wang, L. Huang, R. Yang, Z. Zhang, J. Wu, Y. Gao, Q. Wang, D. OHare and Z. Zhong, *Energy Environ. Sci.*, 2014, **7**, 3478–3518.
11 K. Nakagawa and T. Ohashi, *J. Electrochem. Soc.*, 1998, **145**, 1344.
12 M. Puccini, M. Seggiani and S. Vitolo, *Chem. Eng. Trans.*, 2013, **32**, 1279–1284.
13 Mineral Commodity Summaries, 2015, http://minerals.usgs.gov/minerals/pubs/mcs/2015/mcs2015.pdf, accessed September 2015.
14 J. Ida, R. Xiong and Y. Lin, *Sep. Purif. Technol.*, 2003, **36**, 41.
15 C. Wang, B. Dou, Y. Song, H. Chen, Y. Xuand and B. Xie, *Ind. Eng. Chem. Res.*, 2014, **53**, 12744–12752.
16 P. Subha, B. Nair, P. Hareesh, A. Mohamed, T. Yamaguchi, K. Warrier and U. Hareesh, *J. Phys. Chem. C*, 2015, **119**(10), 5319–5326.
17 M. Seggiani, M. Puccini and S. Vitolo, *Int. J. Greenhouse Gas Control*, 2013, **17**, 25–31.
18 H. Radfarnia and M. Iliuta, *Ind. Eng. Chem. Res.*, 2011, **50**, 9295–9305.
19 M. Bañares, *Catal. Today*, 2005, **100**, 71–77.
20 S. Fung and C. Querini, *J. Catal.*, 1992, **138**, 240–254.
21 T. Hirata, E. Asari and M. Kitajima, *J. Solid State Chem.*, 1994, **110**(2), 201–207.
22 Y. Baklanova, T. Denisova, L. Maksimova, A. Tyutyunnik, I. Baklanova, I. Shein, R. Nederb and N. Tarakina, *Dalton Trans.*, 2014, **43**, 2755.

23 N. Koura, S. Kohara, K. Takeuchi, S. Takahashi, L. Curtiss, M. Grimsditch and M. Saboungi, *J. Mol. Struct.*, 1996, **382**, 163–169.
24 M. Brooker and J. Bates, *J. Chem. Phys.*, 1971, **54**, 4788.
25 S. Kohara, N. Koura, Y. Idemoto, S. Takahashi, M. Saboungic and L. Curtiss, *J. Phys. Chem. Solids*, 1998, **59**(9), 1477–1485.
26 R. Xiong, J. Ida and Y. Lin, *Chem. Eng. Sci.*, 2003, **58**, 4377–4385.
27 E. Ochoa-Fernández, M. Rønning, X. Yu, T. Grande and D. Chen, *Ind. Eng. Chem. Res.*, 2008, **47**, 434–442.
28 S. Zhang, Q. Zhang, C. Shen, Y. Ni, Y. Wu, Q. Wu and Z. Zhu, *Ind. Eng. Chem. Res.*, 2015, **54**(29), 7292–7300.
29 A. Iwan, H. Stephenson, W. Ketchiec and A. Lapkin, *Chem. Eng. J.*, 2009, **146**, 249–258.
30 M. Mizuhata, S. Suganuma and S. Deki, *presented in part at 206th Meeting, © 2004*, The Electrochemical Society, Inc, Honolulu, Hawaii, October, 2004.
31 M. Olivares-Marín, M. Castro-Díaz, T. Drage and M. Maroto-Valer, *Sep. Purif. Technol.*, 2010, **73**, 415–420.